Journal of ELECTRONIC MATERIALS, Vol. 46, No. 11, 2017
DOI: 10.1007/s11664-017-5672-9


# Effects of Forming Processes on the Microstructure and Solderability of Sn-3.5Ag Eutectic Solder Ribbons as well as the Mechanical Properties of Solder Joints

SHENGFA LIU,[1] ZHEBING HU,[1,3] JIERAN XIONG,[2] GUANGHUA TAN,[1] WENYONG XIONG,[1] CHEN CHEN,[1] and SHANGYU HUANG[1]

1.—School of Materials Science and Engineering, Wuhan University of Technology, Wuhan 430070, China. 2.—Shanwei Bolin Electronic Package Material Co., Ltd., Shanwei 516600, China. 3.—e-mail: huzhebing_123@163.com

Two kinds of Sn-3.5Ag eutectic solder ribbons of 0.13 mm thickness were prepared by a casting–rolling process and a rapid solidification process. The microstructure, phase constitution, melting characteristics, wetting behavior and soldering strength were compared using optical microscopy, scanning electron microscopy, x-ray diffraction, energy dispersive spectroscopy, differential scanning calorimetry and a MTS ceramic testing system. The results show that the microstructure of rapidly solidified solder is finer and more uniform, and the eutectic structure has a higher solid solubility and more homogeneous distribution of Ag in a Sn matrix. The solidus and liquidus temperature decreased, resulting in a 3.3% reduction of pasty range. In addition, the wettability and shear strength of the solder joints increased by 13.2% and 7.9%, respectively.

**Key words:** Rapid solidification, Sn-3.5Ag eutectic solder ribbon, microstructure, property

## INTRODUCTION

The recent miniaturization and intelligence trend of electronic products promotes the rapid development of electronic packaging materials.[1,2] The traditional Pb-containing solder has been unable to meet more stringent environmental regulations, requirements for greater mechanical reliability, and increasing demands for high-temperature service environments.[3,4] Therefore, there is an urgent need to replace it with alternative lead-free solders.[5] In particular, a Sn-Ag solder alloy has been recognized as one of the most promising candidates.[6]

The casting–rolling process (CRP) and rapid solidification process (RSP) are frequently used to produce solder ribbons.[7] The CRP is a multi-step process, including casting, rolling, heat treatment, etc. However, the RSP can prepare solder ribbons directly from the melt, and has many advantages such as simple processes, short production cycle, high finished product rate, and good formability of difficult-to-form solder.[8]

Based on the advantages of RSP, only recently have plenty of relevant studies been conducted. Shalaby[9] prepared Sn-3.5Ag lead-free solders by a melt-spinning process and confirmed the formation of $\varepsilon$-$Ag_3Sn$ intermetallic compounds (IMCs) embedded in Sn matrix phase were produced during RSP, and that it was not found under equilibrium conditions. Kamal et al.[10] investigated the effects of RSP on the structure and properties of some lead-free solder alloys and found that RSP caused the formation of some IMCs, such as $Ag_3Sn$ in the Sn-3.5Ag alloy, reduction of the melting points and the measured density, resulting in an increase of the electrical resistivity. Shen et al.[11] obtained lead-free Sn-3.5Ag solders at the cooling rate ranging from 0.08 K/s to $10^4$ K/s and verified that RSP was

(Received February 3, 2017; accepted June 30, 2017; published online July 13, 2017)
The original version of this article has been corrected as reflected in the erratum: In the third paragraph of the Introduction, $Ag_3Snm$ is corrected as $Ag_3Sn$.

of benefit to the formation of fine $\beta$-Sn and spherical $Ag_3Sn$ phases, and improved the microhardness of the Sn-3.5Ag solder. Dutta et al.[12] investigated the impression creep characterization of rapidly cooled Sn-3.5Ag solders, and reported that, in the as-reflowed state, the solder creeps by a viscous glide-controlled mechanism at low stresses due to the supersaturation of Ag in the Sn matrix, and a particle-limited climb mechanism at high stresses. In this work, two kinds of Sn-3.5Ag eutectic solder ribbons were prepared to compare the differences of the microstructure and properties.

## EXPERIMENTAL

In the CRP, the cast ingots were produced by permanent mold casting after melting pure Sn and Ag of purities 99.99% in an electrical furnace under an inert argon atmosphere, and then the solder ribbon of 0.13 mm thickness was prepared by subsequent rolling (Fig. 1a). The other kind of solder ribbon of 0.13 mm thickness was prepared directly by a self-developed rapidly solidified experimental device (Fig. 1b) using the parameters listed in Table I. The two kinds of solder ribbons were cut into 2.8 mm × 3.8 mm rectangular sheets, washed and then dried for subsequent experiments.

The microstructure of the sheets etched with a solution of 5% (volume fraction, the same below) $HNO_3$ + 95%$C_2H_5OH$ was observed using optical microscopy (OM; ECLIPSE LV100POL) and scanning electron microscopy (SEM; Quanta 400).[13] Phase constitutions were determined using x-ray diffraction (XRD; D/Max-RB). Micro-morphology and composition were studied by electron probe microanalysis (EPMA; JXA-8230) and energy dispersive spectroscopy (EDS; Inca X-Act).

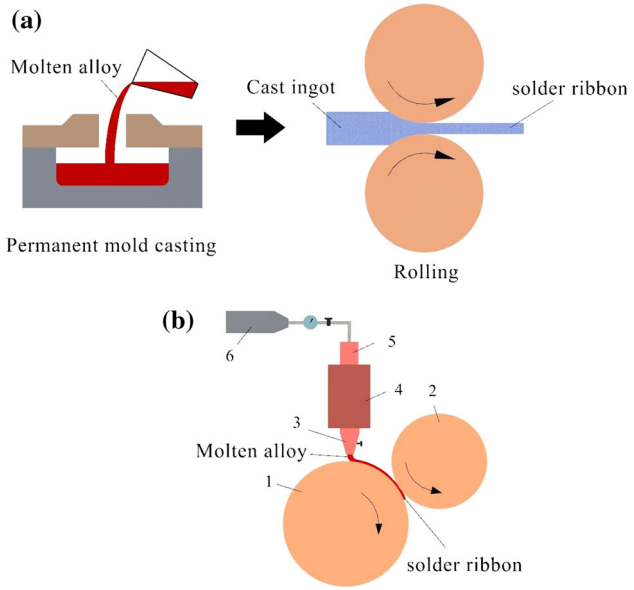


Fig. 1. Schematic diagram of experimental device: (a) CRP, (b) RSP; *1* chilling roller, *2* auxiliary roller, *3* nozzle, *4* heater, *5* crucible and *6* argon gas bomb.

The effects of CRP and RSP on the melting characteristics were studied by differential scanning calorimetry (DSC-PYRIS1) at a constant rate of 10°C/min between 20°C and 250°C under a $N_2$ atmosphere during heating. The wetting behavior was investigated by a spreading experiment carried out on gold-plated substrates at a heating temperature of 230°C with heat insulation time of 60 s under a $N_2$ atmosphere, and then the spreading area was measured using a two-dimensional video measuring system (VMS-1510F). The soldering experiment was carried out with the same parameters as the spreading experiment, and then the shear strength of the solder joints was measured by a MTS ceramic testing system under a tensile shear strain rate of about $3 \times 10^{-4}$ $s^{-1}$ at 20°C in air (Fig. 2). The shear strain was calculated by firstly subtracting the elastic displacement of the gold-plated substrate from the total displacement and then dividing the result by the thicknesses of the solders.[14] Four specimens for each kind of solder joint were tested under the same conditions of experiment to obtain an average value.

## RESULTS AND DISCUSSION

### Microstructure

The optical and SEM microstructure of Sn-3.5Ag eutectic solder alloy by CRP is shown in Fig. 3a–c. The microstructure consists of the white primary $\beta$-Sn phase and gray eutectic structure including $Ag_3Sn$ IMCs and $\beta$-Sn. The primary $\beta$-Sn phase is distributed in coarse dendrites and is surrounded by the eutectic structure (Fig. 3a). The white primary $\beta$-Sn phase is distributed in a banded structure along the rolling direction and surrounded by the gray eutectic structure (Fig. 3b). The primary $\beta$-Sn phase and eutectic structure are distributed in discontinuous bulk and fiber-like, respectively (Fig. 3c). The optical and SEM microstructure of solder alloy by RSP is shown in Fig. 3d and e. The primary $\beta$-Sn phase is distributed in fine equiaxed dendrites and surrounded by an interdendritic eutectic structure (Fig. 3d). The primary $\beta$-Sn phase is distributed in fine equiaxed dendrites and bulk, and surrounded by the eutectic structure distributed in an agglomerate structure. The $Ag_3Sn$ particles in the eutectic mixture are near-spherical in shape with an average size of smaller than 1 $\mu$m in diameter (Fig. 3e). Compared with the microstructure of the casting-rolling solder ribbon (Fig. 3b and c), the primary $\beta$-Sn phase and eutectic structure in a rapidly solidified solder ribbon (Fig. 3d and e) are finer, with a uniform and random distribution.

The XRD diffraction patterns for Sn-3.5Ag eutectic solder ribbons by CRP and RSP are shown in Fig. 4. According to the XRD analysis results, only $\beta$-Sn and $Ag_3Sn$ exist in the solder, showing that the RSP is unable to change the phase constitutions.

**Table I. Process parameters for rapid solidification of the Sn-3.5Ag eutectic solder ribbon of 0.13 mm thickness**

| Thickness (mm) | Heating temperature (°C) | Roller speed (r/min) | Roller distance (mm) | Nozzle–roller distance (mm) | Nozzle size (mm) |
|---|---|---|---|---|---|
| 0.13 ± 0.01 | 230 | 750 | 0.12 | 10 | 0.3 × 20 |

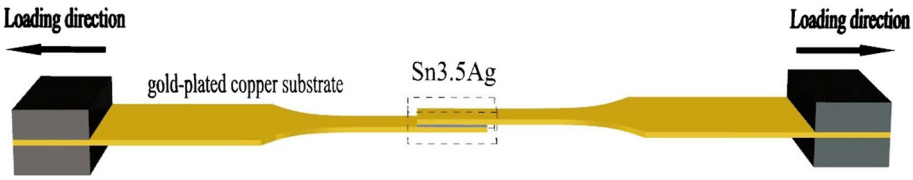


Fig. 2. Schematic diagram of tensile shear strength tests of the solder joints.

The refinement mechanism of primary $\beta$-Sn in rapidly solidified Sn-3.5Ag eutectic solder can be explained by the classical nucleation theory[15]:

$$I = n_s^* \varepsilon v_L n \exp\left(-\frac{\Delta G^*}{kT}\right) \exp\left(-\frac{Q}{kT}\right) \quad (1)$$

where $I$ is the nucleation rate, $n$ is the number of atoms per unit volume of the liquid, $\Delta G^*$ is an activation energy for the nucleation of a critical number of the clustered atoms, $n_s^*$ is the number of atoms on the surface of the critical nucleus, $\varepsilon$ and $v_L$ depend on the activity of atoms, $Q$ is an activation free energy for diffusion across the solid–liquid interface, $k$ is the Boltzman's constant, and $T$ is the thermodynamic temperature. For metals, It is found that the higher the undercooling degree $\Delta T$, the larger the $\Delta G^*$, leading to the increase of $I$. In RSP, the higher solidification rate and larger undercooling degree $\Delta T$ promote the rapid nucleation of the primary $\beta$-Sn phase and reduce the solidification time, resulting in the formation of fine equiaxed dendrites, while, in CRP, the lower solidification rate and smaller $\Delta T$ obtained by permanent mold casting coarsen the dendrite of the primary $\beta$-Sn phase, yielding coarse primary $\beta$-Sn. Moreover, the primary $\beta$-Sn after subsequent rolling is coarser than that in the rapidly solidified solder.

The refinement and uniformity of the eutectic structure are attributed to the higher solidification rate and larger undercooling degree in RSP. The larger undercooling degree firstly crystallizes a large amount of primary $\beta$-Sn phase, bringing about an increase of Ag content in the remaining liquid, i.e., an increase of $n$. According to Eq. 1, $I$ increases with decreasing $n$. Moreover, the higher solidification rate promotes nucleation but suppresses the growth of the $Ag_3Sn$ phase, yielding fine spherical-shaped $Ag_3Sn$ IMCs particles in the Sn matrix.[16] In addition, due to the mismatched crystalline orientation relationships ($Ag_3Sn$ has a facet structure but $\beta$-Sn a non-facet structure), the $Ag_3Sn$ is nucleated separately around the primary $\beta$-Sn phase and hinders the subsequent $\beta$-Sn from attaching to the eutectic $\beta$-Sn, giving rise to the formation of fine dendritic eutectic $\beta$-Sn.[17] The two phases eventually form a finer eutectic structure and the spherical-shaped $Ag_3Sn$ IMCs particles are finely dispersed in the interdendritic regions of eutectic $\beta$-Sn. However, in the CRP, the lower solidification rate and smaller undercooling degree obtained by permanent mold casting suppress the nucleation but promote the growth of the $Ag_3Sn$ phase, yielding coarser $Ag_3Sn$ particles and a eutectic structure. Moreover, the eutectic structure after subsequent rolling is coarser than that in the rapidly solidified solder.[18]

## Solid Solubility and Distribution of Ag Element

Figure 5 shows the distribution of elements in the two kinds of solder ribbons using electron microprobe analysis. The results are listed in Table II. Points $A_1$ and $A_2$ are the Sn matrix without Ag. Points $B_1$ and $C_1$ (Fig. 5a) and points $B_2$ and $C_2$ (Fig. 5d) are of eutectic structure and have Ag contents 3.84 wt.%~4.19 wt.% and 5.61 wt.%~6.91 wt.%, respectively, showing that the solid solubility of Ag in the Sn matrix increases in rapidly solidified solder. Compared with the compositions of the casting–rolling solder (Fig. 5b and c), the compositions of the rapidly solidified solder (Fig. 5e and f) are more uniform. The main reasons are that, in RSP, the higher solidification rate and larger undercooling degree hinder the full diffusion of the solute in liquid and solid, deviatethe solute transport at the solidification interface from the equilibrium, dissolve more solutes into solid, and cause a more significant effect

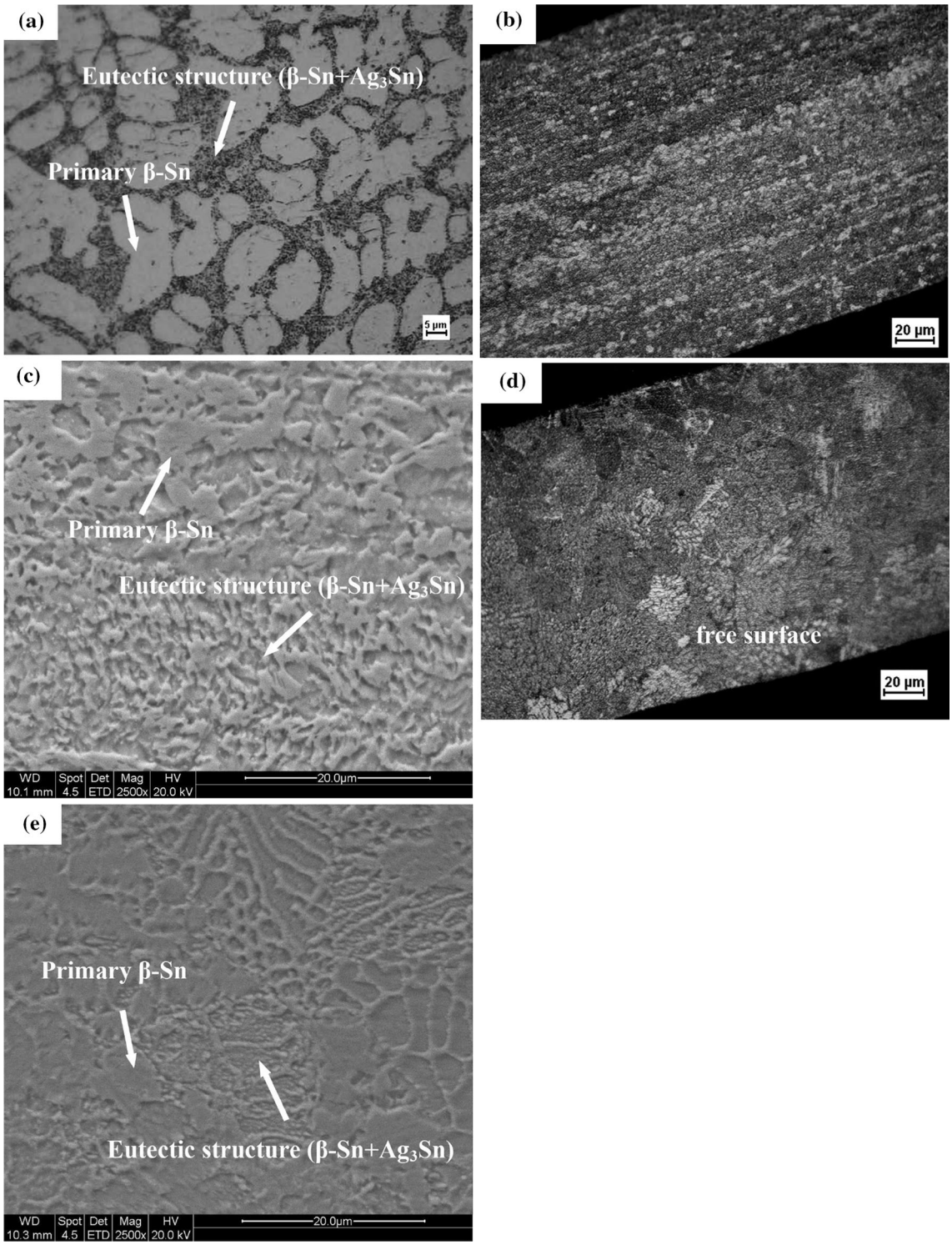


Fig. 3. Microstructure of Sn-3.5Ag eutectic solder alloy by CRP: (a) solder ingot (OM), (b) solder ribbon (OM), (c) solder ribbon (SEM), optical (d) and SEM (e) microstructure of solder ribbon by RSP.

of solute trapping, inducing an increase in the solid solubility of Ag in the Sn matrix and decreasing the Ag segregation.[19] In addition, the fine dendrites improve the solute segregation, leading to the more homogeneous distribution of Ag in the Sn matrix. However, in CRP, due to the lower solid solubility of Ag and coarser dendrites obtained by the permanent mold casting, the Ag segregation after subsequent rolling is higher than that in the rapidly solidified solder.

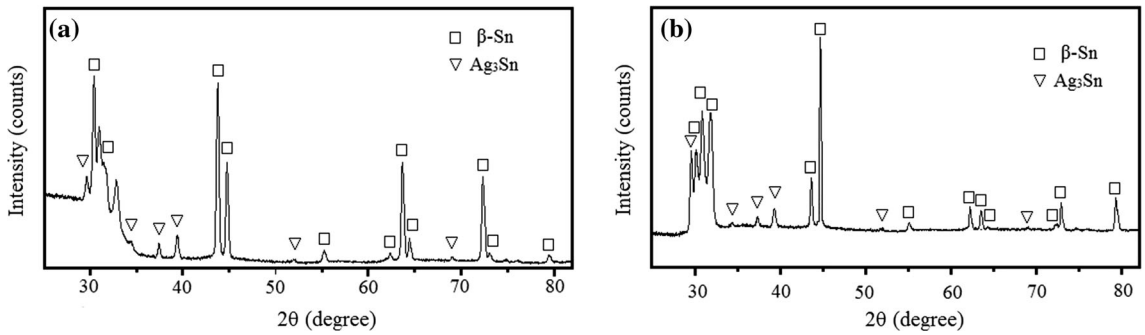


Fig. 4. The XRD patterns of two kinds of Sn-3.5Ag eutectic solder ribbons: (a) CRP and (b) RSP.

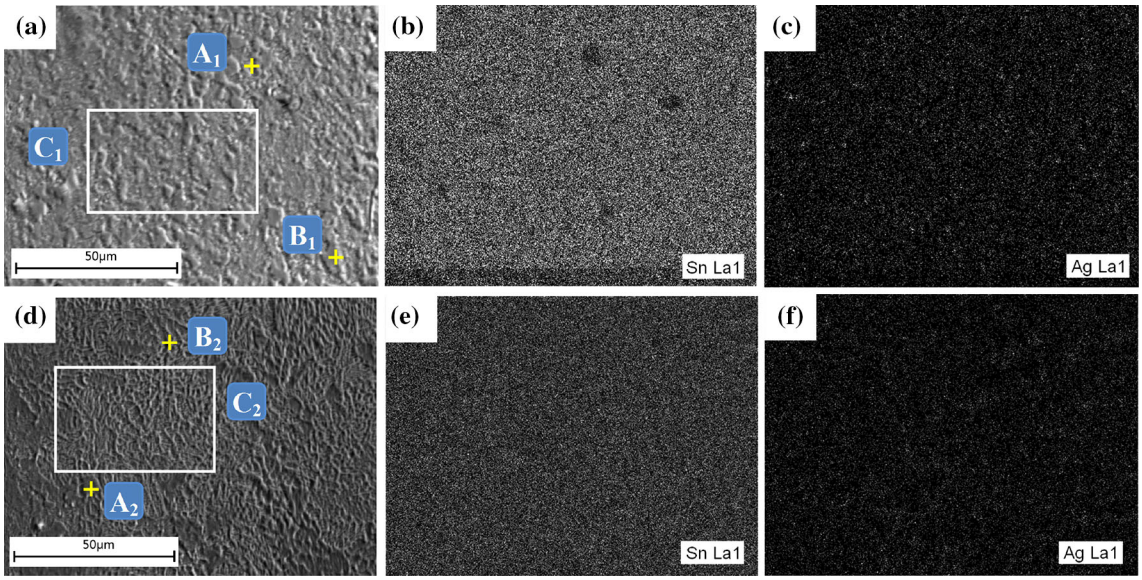


Fig. 5. The electron probe micrograph and element distribution of Sn-3.5Ag eutectic solder ribbons: (a), (b), (c) CRP, (d), (e), (f) RSP.

## Properties

### *Melting Characteristics*

The melting characteristics of the solder ribbons by CRP and RSP were measured using differential scanning calorimetry (DSC). The DSC endothermic peaks of the solders are shown in Fig. 6, and the results are listed in Table III. The solidus and liquidus temperatures decrease from 224.40°C to 223.03°C and from 226.61°C to 225.17°C, respectively, leading to a slight reduction of the corresponding solid–liquid phase temperature difference from 2.21°C to 2.14°C. The main reasons are: (1) the finer microstructure of the rapidly solidified solder increases the specific surface area and surface energy, leading to the decrease of the melting temperature[20]; (2) the microstructure of the rapidly solidified solder is formed by crystallizing under short-range diffusion, and thus can be quickly converted into liquid at a temperature above the melting point; and (3) the higher supersaturation of Ag in the Sn matrix increases the lattice constant of the Sn-based solid solution and interatomic distance and reduces the interatomic force, and thus decreases the melting temperature of the rapidly solidified solder.

### *Wetting Behavior*

Figures 7 and 8 show typical images and average spreading areas of two kinds of Sn-3.5Ag eutectic solder ribbons after the spreading experiment. The average spreading area increases by 13.2%, from 28.1 $mm^2$ to 31.8 $mm^2$. The main reasons are, first, the later melting phase with a high melting point hinders the flow of the earlier melting phase with a low melting point in casting–rolling solder. However, the finer microstructure and more uniform compositions in the rapidly solidified solder decrease the pasty range (the difference between the liquidus and solidus temperatures during the heating process), increase the melting consistency and spreading

**Table II. Chemical analyses at points shown in Fig. 5a and d**

| Process | Test point | Sn (wt.%) | Ag (wt.%) |
|---|---|---|---|
| CRP | $A_1$ | 100.00 | 0.00 |
| | $B_1$ | 95.81 | 4.19 |
| | $C_1$ | 96.16 | 3.84 |
| RSP | $A_2$ | 100.00 | 0.00 |
| | $B_2$ | 93.09 | 6.91 |
| | $C_2$ | 94.39 | 5.61 |

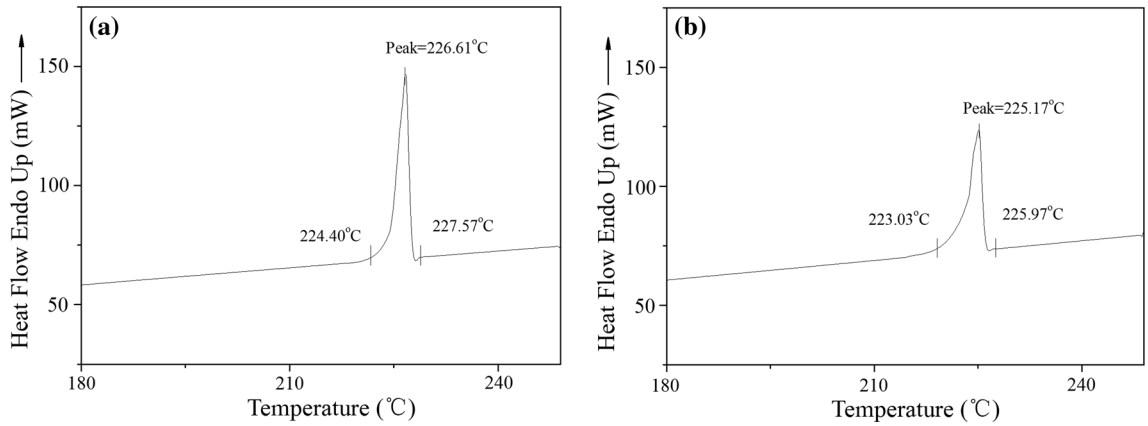


Fig. 6. The differential scanning calorimetry of two kinds of Sn-3.5Ag eutectic solder ribbons: (a) CRP, (b) RSP.

**Table III. Solidus temperature ($T_s$), liquidus temperature ($T_l$) and pasty range of two kinds of Sn-3.5Ag eutectic solder ribbons**

| Process | $T_s$ (°C) | $T_l$ (°C) | Pasty range ($T_l - T_s$) (°C) |
|---|---|---|---|
| CRP | 224.40 | 226.61 | 2.21 |
| RSP | 223.03 | 225.17 | 2.14 |

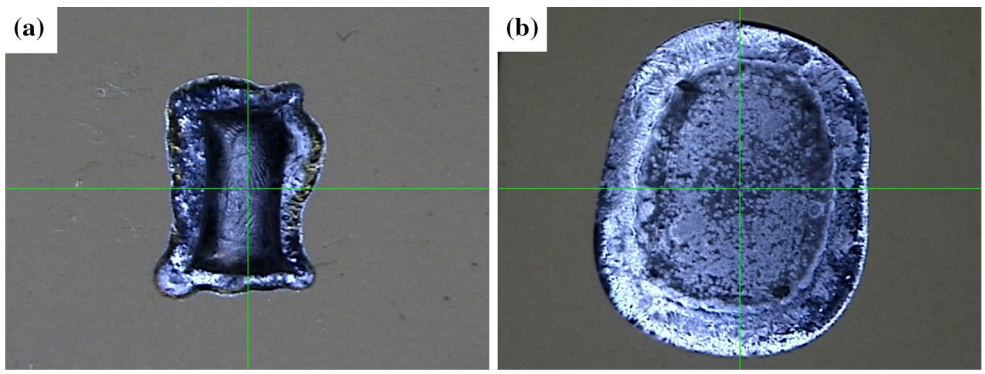


Fig. 7. Typical images of two kinds of Sn-3.5Ag eutectic solder ribbons after the spreading experiment: (a) CRP, (b) RSP.

uniformity, and enhance the wettability.[21] Second, under the same soldering conditions, the lower liquidus temperature of the rapidly solidified solder increases the superheat and fluidity, and thus improves wettability. And, third, the wettability is

determined by the physical wetting effect. According to the Young–Dupre equation[22]:

$$\cos\theta = (\sigma_{SG} - \sigma_{SL})/\sigma_{LG} \quad (2)$$

where $\sigma_{SG}$, $\sigma_{SL}$ and $\sigma_{LG}$ are solid–gas, liquid–solid and gas–liquid surface energy, respectively, and $\theta$ is the wetting angle. The highly reactive atoms in the more uniform and disordered melt of the rapidly solidified solder are easier to combine with the atoms on the substrates, and decrease the surface energy $\sigma_{SL}$ and wetting angle $\theta$, and thus increase the wettability.

*Shear Strength*

The schematic diagrams for two kinds of solder joints and brittle fracture mode are shown in Fig. 9. The typical shear stress–strain curves of the solder joints are shown in Fig. 10. The average shear strengths of casting–rolling and rapidly solidified solder joints are shown in Fig. 11. The average shear strength increases by 7.9% from 32.65 ± 0.80 MPa to 35.23 ± 0.50 MPa. The main reasons are that the coarser and strongly directional microstructure is not beneficial for enhancing the shear strength of casting–rolling solder joints, while the finer and more uniform microstructure with finely dispersed $Ag_3Sn$ IMCs particles contributes to the improvement of the shear strength of the rapidly solidified solder joints.

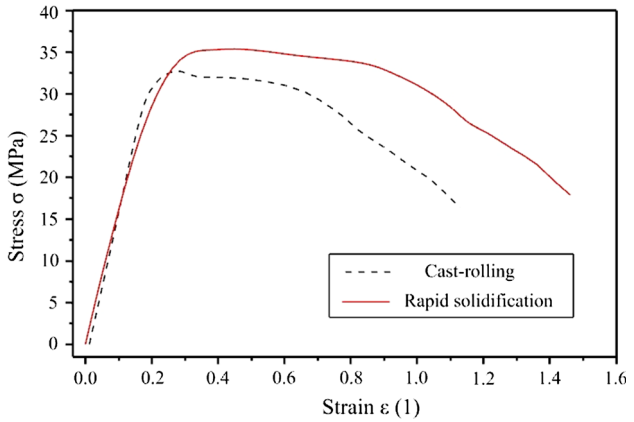


Fig. 10. Typical stress–strain curves of casting–rolling and rapidly solidified solder joints.

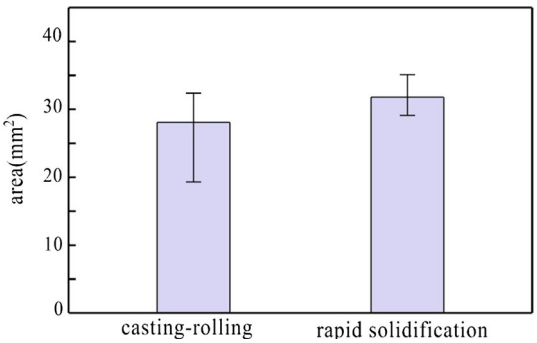


Fig. 8. The wettability of two kinds of Sn-3.5Ag eutectic solder ribbons.

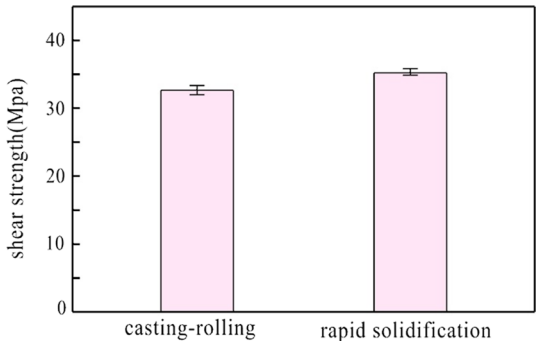


Fig. 11. The average shear strength of casting–rolling and rapidly solidified solder joints.

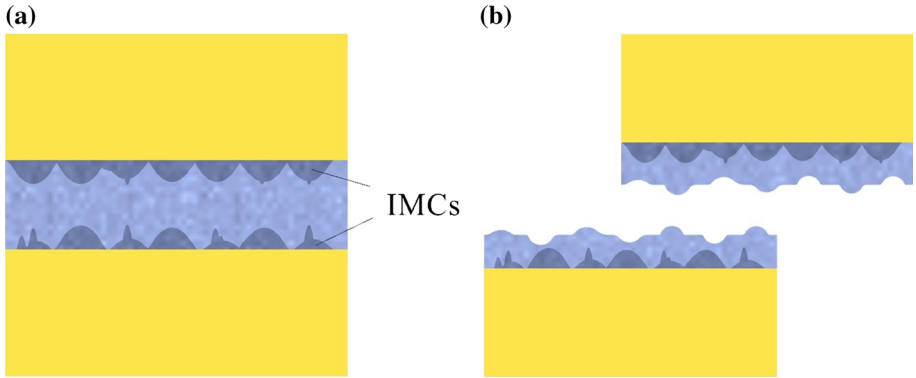


Fig. 9. The schematic diagrams of the solder joints (a), brittle fracture (b).

## CONCLUSIONS

(a) Compared with CRP, the higher cooling rate and larger undercooling degree obtained by RSP cause the refinement and uniformity of the primary $\beta$-Sn and eutectic structures, strengthen the effect of solute trapping, and increase the solid solubility and uniformity of Ag in the Sn matrix.
(b) Compared with casting–rolling solder, the finer and more uniform microstructure of rapidly solidified Sn-3.5Ag eutectic solder ribbons decreases the solidus temperature and pasty range, and improves the wettability. In addition, the shear strength increases due to the finely dispersed distribution of $Ag_3Sn$ IMCs particles in the rapidly solidified solder joints.

## ACKNOWLEDGEMENT

The authors would like to express their thanks to the National Natural Science Foundation of China (Grant No. 51475345).

## REFERENCES

1. M. Sobhy, A.M. El-Refai, M.M. Mousa, and G. Saad, *Mater. Sci. Eng. A* 646, 82 (2015).
2. G. Chen, F. Wu, C. Liu, V.V. Silberschmidt, and Y.C. Chan, *J. Alloys Compd.* 656, 500 (2016).
3. M. Abtew and G. Selvaduray, *Mater. Sci. Eng. R* 27, 95 (2000).
4. E.H. Amalu and N.N. Ekere, *J. Mater. Process. Technol.* 212, 471 (2012).
5. W.R. Osório, D.R. Leiva, L.C. Peixoto, L.R. Garcia, and A. Garcia, *J. Alloys Compd.* 562, 194 (2013).
6. K.S. Kim, S.H. Huh, and K. Suganuma, *Mater. Sci. Eng. A* 333, 106 (2002).
7. E.J. Lavernia and T.S. Srivatsan, *J. Mater. Sci.* 45, 287 (2010).
8. H. Jones, *Mater. Sci. Eng. A* 304, 11 (2001).
9. R.M. Shalaby, *J. Alloys Compd.* 505, 113 (2010).
10. M. Kamal and E.S. Gouda, *Mater. Manuf. Process.* 21, 736 (2006).
11. J. Shen, Y.C. Liu, and J.Y. Han, *Trans. Nonferrous Met. Soc. China* 16, 59 (2006).
12. I. Dutta, C. Park, and S. Choi, *Mater. Sci. Eng. A* 379, 401 (2004).
13. T. Luo, Z. Chen, A. Hu, and M. Li, *Mater. Sci. Eng. A* 556, 885 (2012).
14. Q.K. Zhang, W.M. Long, X.Q. Yu, Y.Y. Pei, and P.X. Qiao, *J. Alloys Compd.* 622, 973 (2015).
15. J. Shen, Y. Liu, Y. Han, and H. Gao, *Rare Met.* 25, 365 (2006).
16. H.T. Lee and Y.F. Chen, *J. Alloys Compd.* 509, 2510 (2011).
17. U.R. Kattner and W.J. Boettinger, *J. Electron. Mater.* 23, 603 (1994).
18. J. Shen, Y.C. Liu, H.X. Gao, C. Wei, and Y.Q. Yang, *J. Electron. Mater.* 34, 1591 (2005).
19. M.J. Aziz, *J. Appl. Phys.* 53, 1158 (1982).
20. X.Y. Li, F.Q. Zu, W.L. Gao, X. Cui, L.F. Wang, and G.H. Ding, *Appl. Surf. Sci.* 258, 5677 (2012).
21. H.T. Ma, J. Wang, L. Qu, N. Zhao, and A. Kunwar, *J. Electron. Mater.* 42, 2686 (2013).
22. T. Young, *Philos. Trans. R. Soc. Lond.* 95, 65 (1805).